Physics-Informed Generalizable Framework Bridges the Sim-to-Real Gap in AI-based Cerebrovascular Hemodynamics Modeling

Supplementary information

Supplementary Notes

Supplementary Figures

Supplementary Notes

1. Data collection protocols

Study Population and Ethics

This study was conducted at the Medical Imaging Diagnostic Center, Shanghai Imagingrace (Shanghai, China) and was approved by the Institutional Review Board of Fuwai Hospital Shenzhen, Chinese Academy of Medical Sciences (Approval No. SP2024095(01)). Written informed consent was obtained from all participants. A total of 40 subjects were randomly recruited for the study; detailed demographic information is provided in Supplementary Table 1.

MRI Acquisition Protocol

Multi-sequence MRI data were acquired using a 3.0 T scanner (uMR Omega, United Imaging Healthcare, Shanghai, China) with a maximum gradient slew rate of 200 T/m/s and a gradient strength of 45 mT/m. Subjects were positioned supine with the mandible slightly elevated to expose the bilateral carotid regions. The scan plane was centered at the carotid artery bifurcation with axial slices perpendicular to the vessel lumen.

High-resolution images of the head and neck vasculature were first collected using a 3D Time-of-Flight (TOF) MRA sequence to enable the 3D reconstruction of cerebrovascular artery geometry. The acquisition parameters were as follows: repetition time (TR) = 18.3 ms; echo time (TE) = 3.5 ms; flip angle (FA) = 16°; field of view (FOV) = 224 × 180 mm^2; matrix = 320 × 100; 4 slabs with 30 slices per slab; slice thickness = 1.4 mm; number of excitations (NEX) = 1; and bandwidth = 350 Hz/pixel. Scan duration and spatial resolution varied by segment: head (2:11 min, 0.7 × 0.7 × 1.1 mm^3), neck (2:57 min, 0.7 × 0.7 × 1.4 mm^3), and chest (3:08 min, 0.75 × 0.75 × 1.6 mm^3).

Subsequently, *in-vivo* blood velocity fields were acquired using a 4D Flow MRA sequence with the following settings: TR = 33.4 ms; TE = 3.76 ms; FA = 8°; FOV = 217 × 225 mm^2; matrix = 240 × 100; 4 slabs with 60 slices per slab; slice thickness = 0.9 mm; NEX = 1; and bandwidth = 350 Hz/pixel. The sequence utilized an isotropic voxel size of 0.6 × 0.6 × 0.6 mm^3, a temporal resolution of 20 frames per cardiac cycle, and a velocity encoding (VENC) of 110 cm/s. The total scan duration for 4D Flow was approximately 9:35 min.

Doppler Ultrasound Acquisition

Patient-specific velocity waveforms were measured using Doppler ultrasonography (Affiniti 30, Philips, USA). Measurements included the bilateral common and internal carotid artery velocity waveforms.

2. Generation process of patient-specific CFD Data

The generation of patient-specific Computational Hemodynamic Data is a multi-stage workflow that transforms clinical medical images into high-fidelity, time-resolved flow fields (Supplementary Fig. 17). The process is outlined as follows.

(1) 3D Geometry Reconstruction: The acquired images collected from 3D Time-of-Flight (TOF) Magnetic Resonance Angiography (MRA) are processed using segmentation software (Materialise Mimics Innovation Suite Research 21.0) to isolate the lumen (the

inner channel) of the target blood vessels (e.g., the carotid artery) from the surrounding tissues. The segmented region is converted into a 3D, watertight surface model, which digitally represents the anatomical geometry as Common Carotid Artery (CCA), Internal Carotid Artery (ICA), External Carotid Artery (ECA) and Vertebral Artery (VA), with the existing mask threshold values range from 250 GV to 750 GV. Using software (Materialise 3-Matic Research 13.0), employed to optimize the three-dimensional models generated in Mimics Research by repairing defects such as holes, geometric flaws, and redundant surfaces. In addition, the three-dimensional mesh is edited to refine structural details, thereby improving the overall accuracy and quality of the model and then converting into STL format for subsequent processing and application.

(2) Mesh Generation: The 3D surface model is imported into a meshing tool (Geomagic Wrap v2021.2.2), in which the STL file contents are converted into a geometrically usable three-dimensional model to support further analysis, modification, and application. The fluid domain (the space inside the vessels where blood flows) is discretized into a large number of small, interconnected elements, such as tetrahedra or polyhedra, to form computational surface patches,with the following parameter settings: surface patches: CCA: 1000s, ECA: 1500s, ICA: 1500s, and VA : 3000s. Subsequently, a structured mesh is generated on each surface of the model. The resolution used for mesh generation is specified as 20. The mesh is typically refined near the vessel walls and in regions of complex geometry to accurately capture high velocity gradients and wall shear stresses. The mesh size is non-uniform, with the maximum element edge length not exceeding 0.45 mm.

(3) Definition of Fluid Properties and Boundary Conditions: Blood is modeled as an incompressible, Newtonian fluid with a constant density of $1060 kg/m^3$ and different viscosity of $0.00277/0.00345/0.00413 Pa \cdot s$ for larger arteries. A patient-specific, time-varying velocity waveform—obtained from Doppler Ultrasound measurements at the common carotid artery—is prescribed at the inlet(s) of the model. The outlet(s) are signed Windkessel R-C-R models that mimic the resistance and compliance of the downstream vasculature.

(4) CFD Simulation: The meshed geometry and boundary conditions are processed using ANSYS Fluent 2025, a CFD software based on the finite volume method. A pressure-based solver and a transient laminar flow model were employed during the simulations. The laminar flow model iteratively computes the numerical solution to the governing Navier-Stokes equations, which describe the conservation of mass and momentum for fluid flow. The simulation time step was set to 0.002 s, with a maximum of 50 iterations per time step to ensure that the residuals reached the prescribed threshold of 1×10^{-3}. Results were exported every 25 time steps, corresponding to a time interval of 0.05 s.

(5) Post-processing and Data Extraction: Once converged, the results are post-processed to extract full, time-varying 3D hemodynamic fields including Velocity (vector field) and Pressure. The final output is a comprehensive, spatio-temporal dataset that represents the simulated hemodynamics within the patient's specific anatomy.

3. Post-processing of 4D MRI data

Raw 4D-flow MRI data were reconstructed into time-resolved 4D datasets (three spatial dimensions plus time), comprising both anatomical magnitude and phase-contrast velocity images. Post-processing was performed using iTFlow software (Cardio Flow Design Inc., Japan). Key steps included phase unwrapping to correct velocity aliasing and noise filtering to enhance data quality. The three directional velocity components were then synthesized into a time-resolved 3D velocity vector field. Following vascular segmentation based on the magnitude images, quantitative hemodynamic parameters, including the velocity field and wall shear stress (WSS), were derived. Finally, the digitized flow fields were exported in .vtk format for downstream analysis (Supplementary Fig. 18).

4. Implemental details of 4DHemoFormer framework

The proposed 4DHemoFormer framework incorporates several tailored architectural designs to optimize performance for fluid dynamics tasks. First, two separate Multilayer Perceptron (MLP) networks encode the flow field features and spatiotemporal information, respectively; their outputs are then summed to generate the input embeddings. The encoder module consists of a four-layer Transformer architecture. To enhance training stability and convergence, it adopts Pre-Layer Normalization (Pre-LN). Additionally, the standard ReLU is replaced with the Sigmoid Linear Unit (SiLU) activation function, which provides smooth differentiability and gradient stability, thereby effectively capturing spatiotemporal dependencies across diverse cases and time frames. For the decoding phase, an MLP-based structure is utilized. This decoder performs direct feature decoding for single-step predictions, whereas for multi-step tasks, it integrates cross-temporal features to facilitate long-term flow field forecasting. Finally, model training is governed by a hybrid loss function, combining a data-driven loss with a physics-informed loss derived from the incompressible Navier-Stokes equations to enforce physical constraints. Detailed architectural hyperparameters and training settings are provided in Supplementary Table 8.

5. Setup of baseline methods

The PINN, DeepONet and FNO are compared with our model on the 4DHemoDB to validate the temporal extrapolation, cross-geometry generalization performance. The experimental setups are listed below:

The implementation of PINN using fully-connected neural networks (FNN) is based on the open-source Python library DeepXDE, with parameters detailed in Supplementary Table 8. The pipeline of training FNO and DeepONets is based on the open-source Python code provided in CFDBench[47]. All hyperparameter optimization strategies for baseline methods follow the same settings used in CFDBench. Specifically, for FNO, DeepONets, we use the Adam optimizer with a learning rate of 10^{-3}, combined with a learning rate schedular that cuts the learning rate by 0.9 every 20 epochs. The FNO and DeepONets are designed for voxel data. To address the irregularity of hemodynamic data, we firstlty employed a voxelization strategy before modeling. The voxelization process involves three key steps. (1) Space Partitioning: A 3D bounding box is defined to encapsulate the region of vascular geometry. (2)Grid Generation: This space is

subdivided into a regular grid of discrete cubic elements with a predefined resolution of 80×120×210; (3) Feature Assignment: Input data points are mapped to their corresponding voxels. For each voxel, a specific value is assigned by aggregating the features of the points falling within it via average pooling. Other detailed hyperparameters of network architecture and the settings for DeepONet and FNO are listed in Supplementary Table 8.

6. Runtime evaluation

To assess computational efficiency, we evaluated the training and inference time of 4DHemoFormer, baseline deep learning models (including FNO, DeepONets, and PINNs), and a full-order model (numerical simulation) across all tasks. For the full-order model, the reported computational time denotes the assimilation time required by a conventional numerical solver coupled with an ensemble-based variational data assimilation technique[s1,s2]—a robust approach widely adopted for complex dynamical systems. Notably, because numerical simulations necessitate well-posed boundary conditions and sufficient grid resolution to ensure convergence, the execution time for the full-order model was benchmarked using the identical spatiotemporal grid and numerical setup employed to generate the training data. Numerical simulations were executed on a Windows 11 (24H2) workstation powered by an AMD Ryzen 7 9700X processor (5.5 GHz maximum clock speed). All computations utilized double-precision floating-point arithmetic (FP64) to guarantee high-fidelity results.

All training and testing were conducted on a single Linux server (Ubuntu 24.04.3 LTS) equipped with an Intel Xeon Platinum 8468 CPU and an NVIDIA H100 GPU (Driver Version: 550.163.01, CUDA Version: 12.4). The computational times are detailed in Supplementary Table 7.

Supplementary Figures

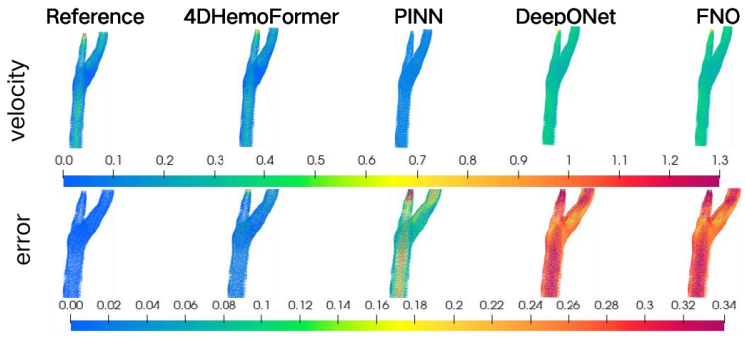

Supplementary Fig. 1. | Performance of temporal extrapolation in single-step prediction task. Comparison between the hemodynamic velocity fields learned and the reference, using CCA as the example.

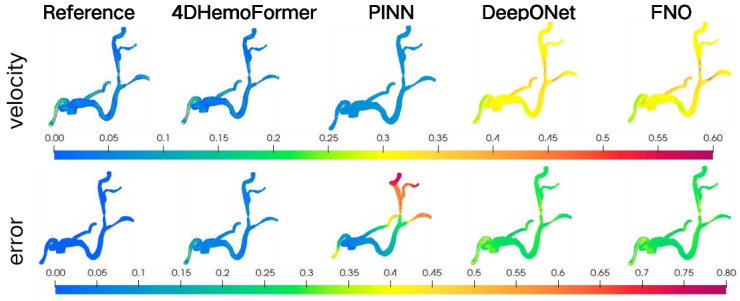

Supplementary Fig. 2. | Performance of temporal extrapolation in single-step prediction task. Comparison between the hemodynamic velocity fields learned and the reference, using ECA as the example.

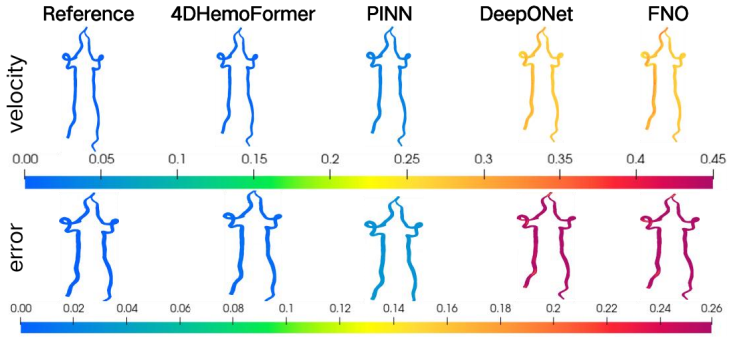

Supplementary Fig. 3. | Performance of temporal extrapolation in single-step prediction task. Comparison between the hemodynamic velocity fields learned and the reference, using VA as the example.

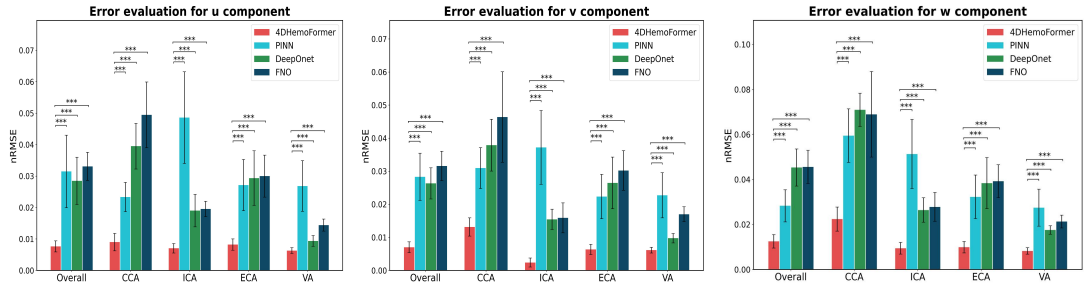

Supplementary Fig. 4. | Performance of temporal extrapolation in single-step prediction task. Comparison of the average performance in terms of nRMSE of the 4DHemoFormer with 3 baseline architectures for individual velocity components. The error bars represent the mean values±std., calculated from the method's predictions across the test dataset. ***p<0.001.

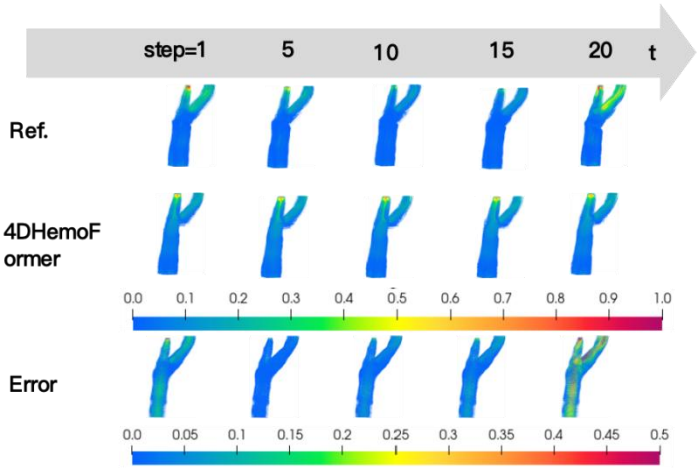

Supplementary Fig. 5. | Performance of temporal extrapolation in multi-step prediction task. Comparison between the hemodynamic velocity fields learned and the reference, using CCA as the example. From up to bottom, the panels represent the numerical simulation (denoted as Ref.), the 4DHemoFormer predictions, and the relative error with time steps.

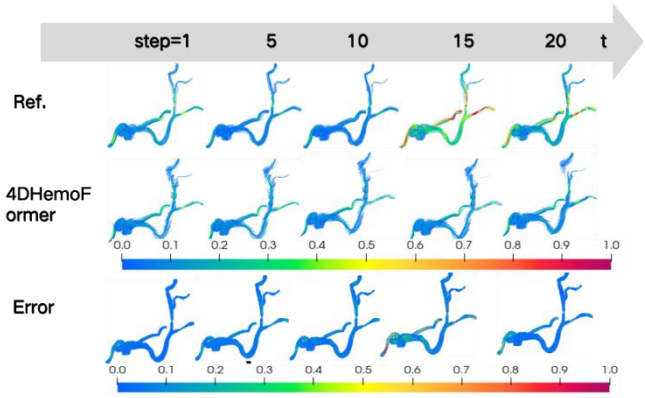

Supplementary Fig. 6. | Performance of temporal extrapolation in multi-step prediction task. Comparison between the hemodynamic velocity fields learned and the

reference, using ECA as the example. From up to bottom, the panels represent the numerical simulation (denoted as Ref.), the 4DHemoFormer predictions, and the relative error with time steps.

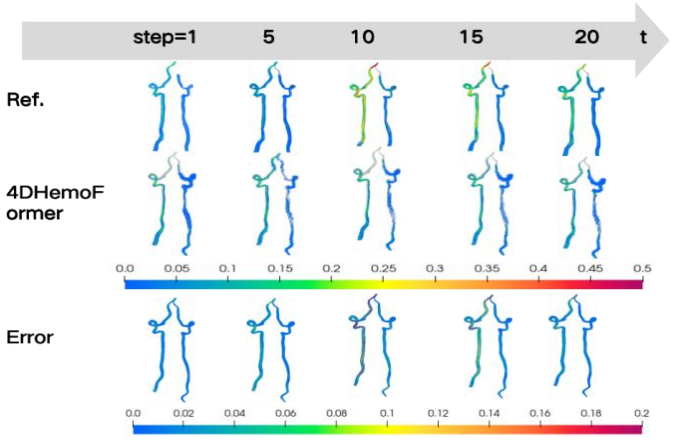

Supplementary Fig. 7. | Performance of temporal extrapolation in multi-step prediction task. Comparison between the hemodynamic velocity fields learned and the reference, using VA as the example. From up to bottom, the panels represent the numerical simulation (denoted as Ref.), the 4DHemoFormer predictions, and the relative error with time steps.

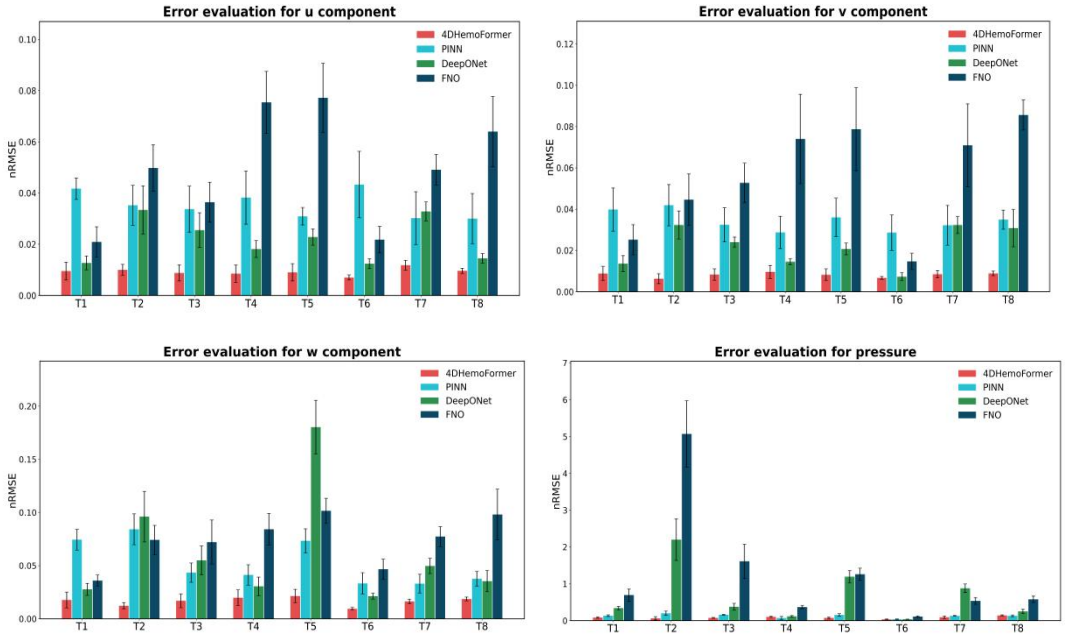

Supplementary Fig. 8. | Performance of temporal extrapolation in multi-step prediction task. Comparison of the average performance in terms of nRMSE of the 4DHemoFormer with 3 baseline architectures for individual velocity components and pressure field. The error bars represent the mean values±std., calculated from the method's predictions across the test dataset. ***p<0.001.

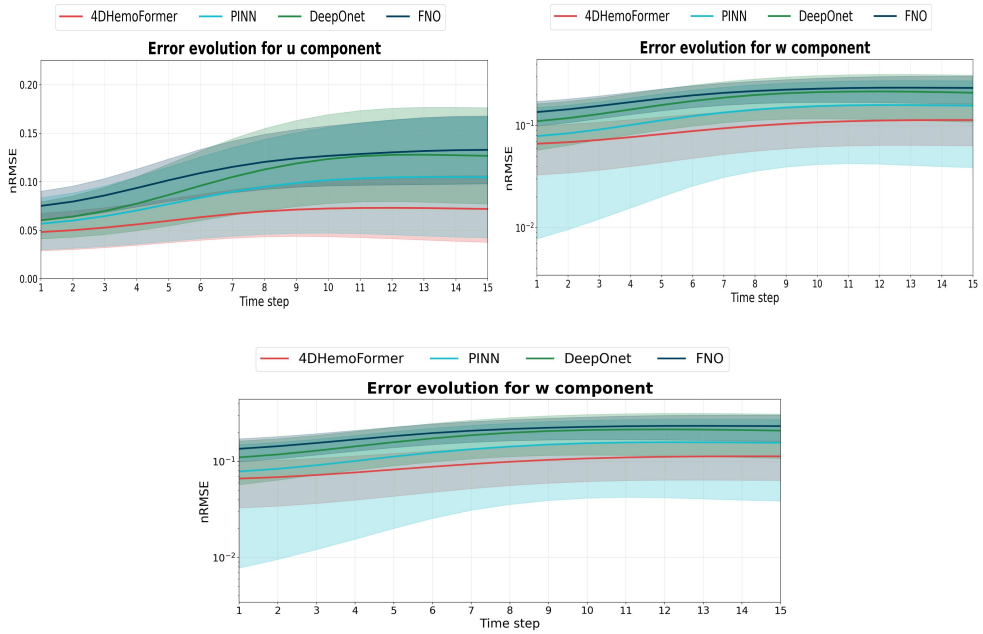

Supplementary Fig. 9. | Performance of temporal extrapolation in multi-step prediction task. Temporal error propagation for individual velocity components predictions in terms of nRMSE. Shaded region represent the variance band.

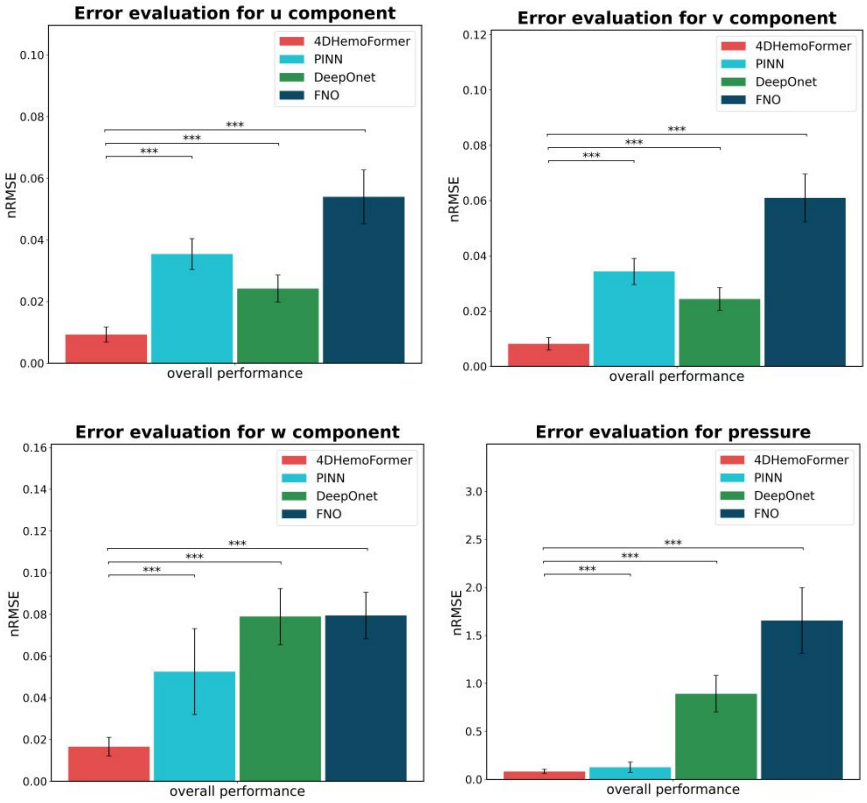

Supplementary Fig. 10. | Performance for cross-geometry generalization in single-step prediction task. Overall performance evaluation of 4DHemoFormer and baselines on 8 cross-geometry tasks in terms of nRMSE for individual velocity

component and pressure component. The bar graph indicates the mean±std. ***p<0.001.

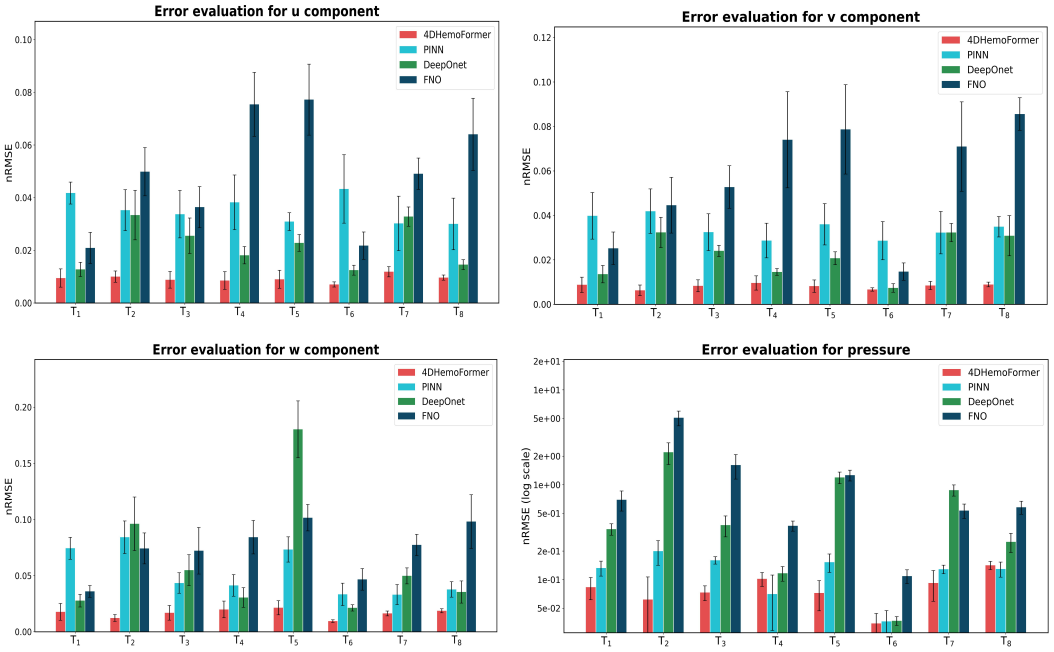

Supplementary Fig. 11. | Performance for cross-geometry generalization in single-step prediction task. Detailed evaluation of 4DHemoFormer and baselines for individual velocity and pressure component on each cross-geometry task.

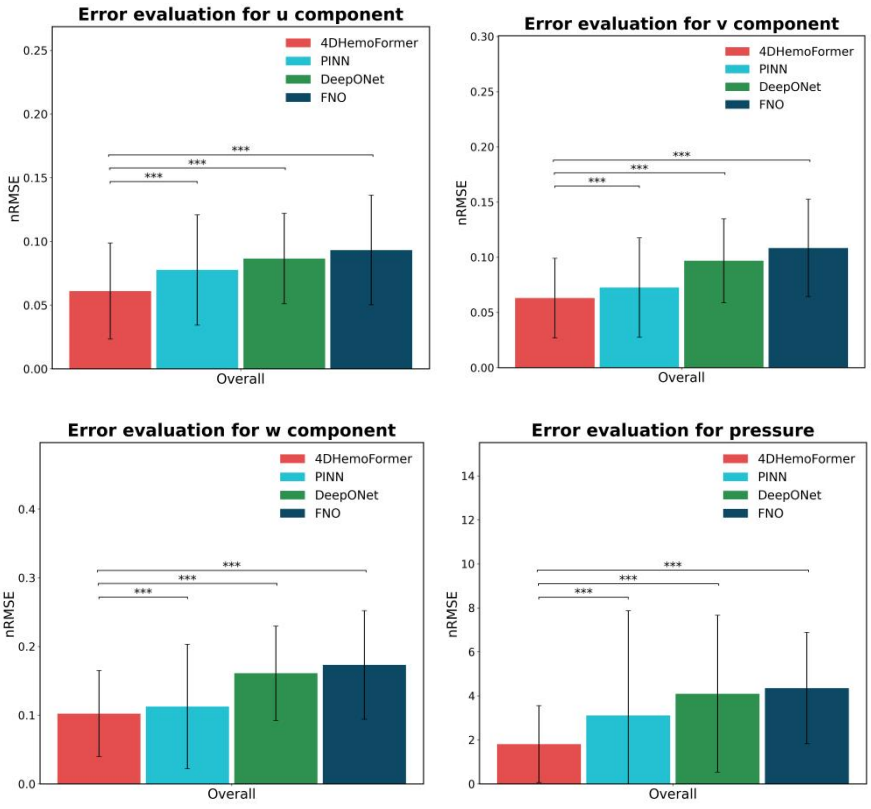

Supplementary Fig. 12. | Performance for cross-geometry generalization in multi-step prediction task. Overall performance evaluation of 4DHemoFormer and baselines for individual velocity and pressure component on 8 cross-domain tasks in terms of nRMSE. The bar graph indicates the mean±std. ***P<0.001.

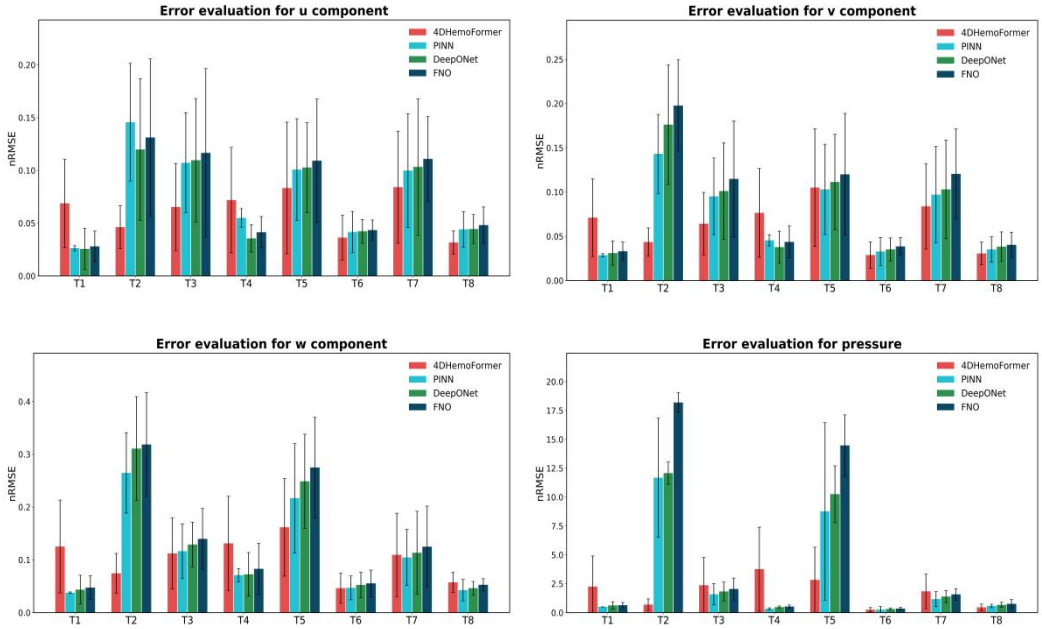

Supplementary Fig. 13. | Performance for cross-geometry generalization in multi-step prediction task. Detailed evaluation of 4DHemoFormer and baselines for individual velocity and pressure component on each cross-geometry task.

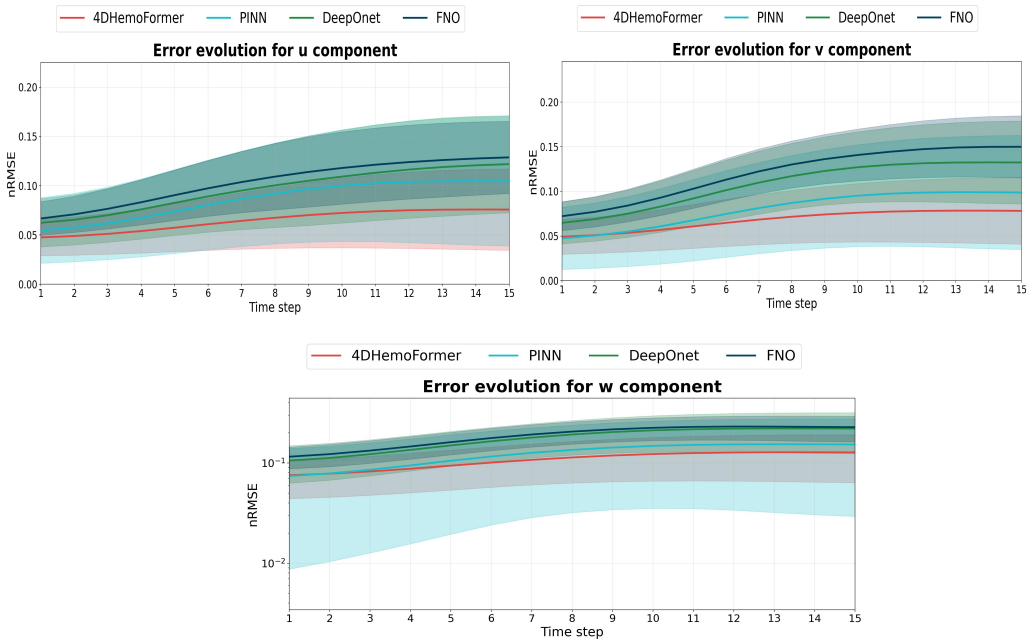

Supplementary Fig. 14. | Performance for cross-geometry generalization in multi-step prediction task. Temporal error propagation for individual velocity components predictions.

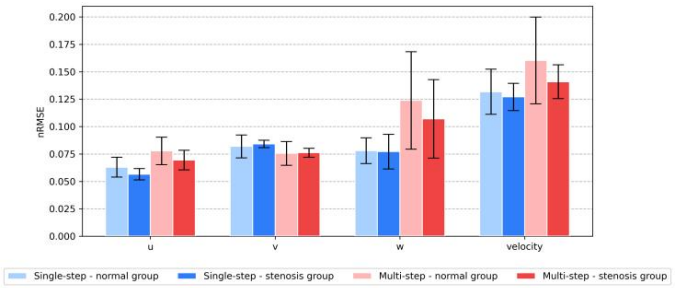

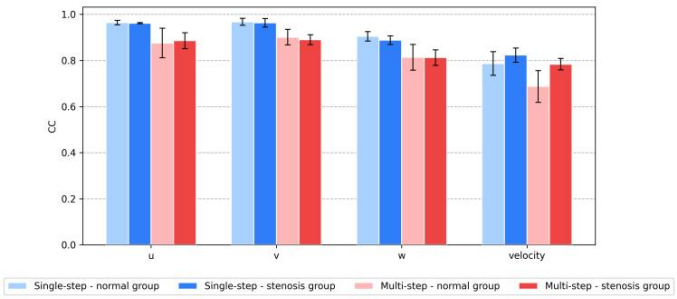

Supplementary Fig. 15. | Comparison of the model's accuracy between the normal and stenosed groups in terms of nRMSE and correlation coefficient.

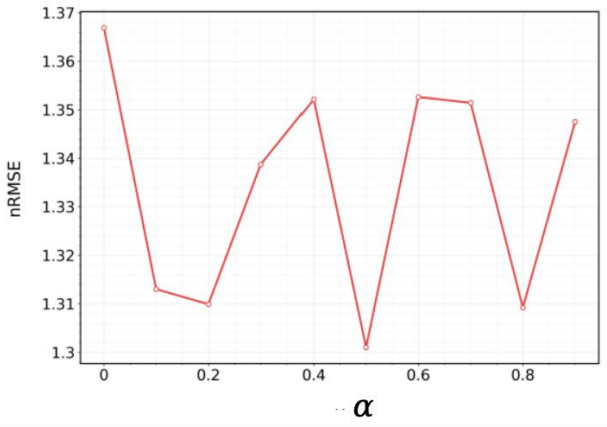

Supplementary Fig. 16. | Impact of physics loss weight, using temporal extrapolation in single-step prediction task as the example.

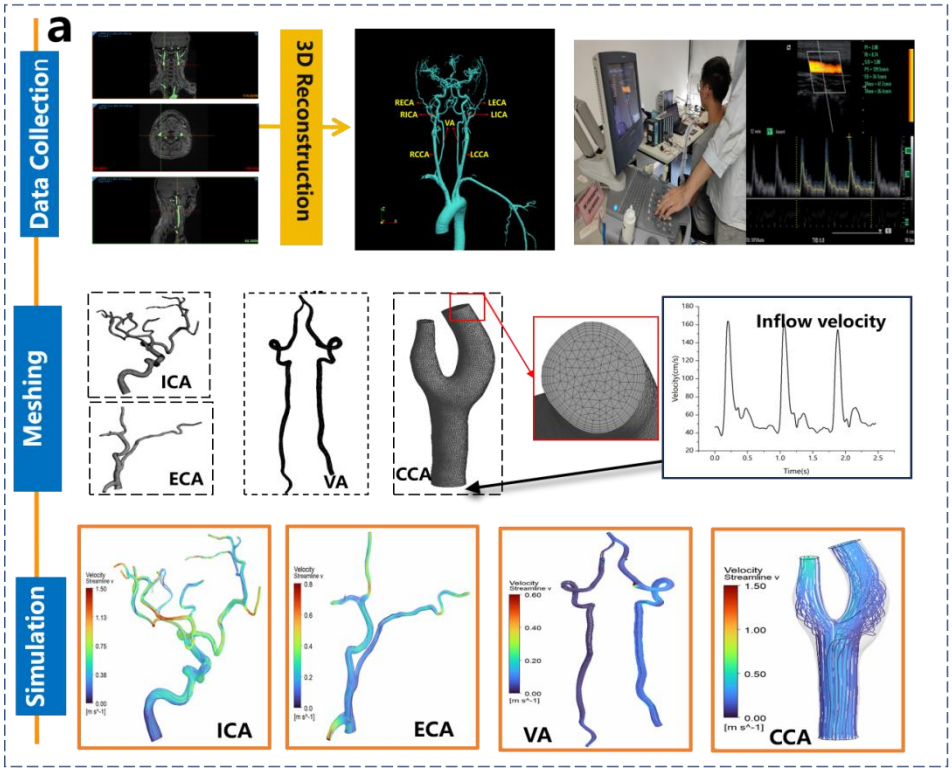

Supplementary Fig. 17. | The workflow of construction process of the CFD dataset. It includes the data collection, meshing and numerical simulation process. LCCA, left common carotid artery; RCCA, right common carotid artery; LICA, left internal carotid artery; RICA, right internal carotid artery; LECA, left external carotid artery; RECA, right external carotid artery; VA, Vertebral artery.

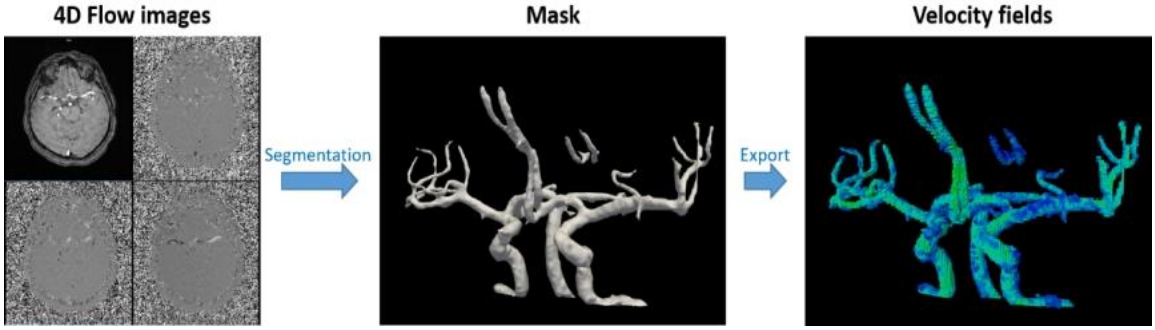

Supplementary Fig. 18. | Post-processing of the 4D Flow images using iTFlow.

Supplementary Tables

Supplementary Table 1. Subject information

	Total (N=40)	Males (N=14)	Females (N=26)
Age (Years)	49[32.5,58]	52.5[33,56]	45[32.5,60.5]
SBP (mmHg)	116[107.5,125.5]	120.5[116,126]	113[105,122]
DBP (mmHg)	74[67.5,80.5]	79[73,83]	69[66,80]
Pulse rate (bpm)	69[63,74.5]	63.5[59,71]	70[66,80]
Carotid artery stenosis (n)	7	4	3

Supplementary Table 2. Prediction Performance (mean+/-std) for single-step prediction task on temporal extrapolation

Vessel Site	**Metrics**	**Models**	**p (10^{-2})**	**u(10^{-2})**	**v(10^{-2})**	**w(10^{-2})**	**velocity magnitude (10^{-2})**
Overall	nRMSE	4DHemoFormer	6.30±2.20	0.76±0.17	0.70±0.16	1.20±0.30	1.70±0.39
		PINN	7.30±5.30	3.10±1.20	2.80±0.71	2.80±0.71	6.80±2.30
		DeepONet	7.82±6.27	2.80±0.75	2.60±0.47	4.50±0.82	6.00±1.70
		FNO	8.39±6.84	3.30±0.45	3.20±0.45	4.60±0.74	6.20±1.50
	Correlation coefficient	4DHemoFormer	80.06±13.26	91.74±3.53	91.90±3.39	92.73±2.00	92.44±2.12
		PINN	74.47±13.59	78.27±13.99	78.03±20.89	78.36±15.89	69.08±17.90
		DeepONet	78.27±14.59	87.25±15.99	85.85±11.06	89.41±19.27	85.25±9.21
		FNO	76.29±18.73	86.87±22.18	86.58±11.95	87.72±13.60	83.94±8.86
CCA	nRMSE	4DHemoFormer	8.00±1.71	0.90±0.28	1.31±0.28	2.24±0.54	2.87±0.61
		PINN	13.02±2.60	2.33±0.47	3.09±0.62	5.95±1.19	6.58±1.32
		DeepONet	18.94±3.28	3.95±0.73	3.79±0.78	7.09±0.74	7.97±1.15
		FNO	16.24±2.73	4.95±1.05	4.64±1.37	6.89±1.90	7.83±1.38
	Correlation coefficient	4DHemoFormer	89.90±28.31	85.41±10.18	85.54±9.78	90.67±4.98	90.91±5.83
		PINN	72.65±24.43	63.45±9.52	48.04±7.21	57.49±8.62	49.23±7.39
		DeepONet	74.79±26.74	83.02±13.55	83.21±22.24	85.44±17.88	84.66±8.80
		FNO	59.87±5.49	82.89±9.64	83.58±17.04	88.56±12.52	87.72±19.39
ICA	nRMSE	4DHemoFormer	0.50±0.20	0.70±0.15	0.24±0.14	0.94±0.26	0.52±0.34
		PINN	0.63±0.19	4.86±1.46	3.72±1.12	5.13±1.54	10.10±3.03
		DeepONet	12.88±2.99	1.90±0.52	1.54±0.31	2.64±0.55	3.51±0.44

		FNO	17.43±2.34	1.95±0.24	1.59±0.45	2.78±0.64	3.72±0.76
		4DHemoFormer	90.57±6.39	95.76±1.92	96.43±1.41	95.77±1.34	95.92±1.02
		PINN	88.92±4.45	71.46±3.57	89.25±4.46	86.17±4.31	73.02±3.65
	Correlation coefficient	DeepONet	85.48±16.60	86.36±17.15	86.54±22.79	86.37±17.28	86.31±21.58
		FNO	85.52±24.67	89.60±26.40	89.78±13.94	89.52±23.60	89.54±21.17
		4DHemoFormer	7.34±3.97	0.82±0.18	0.63±0.15	0.99±0.26	2.07±0.41
		PINN	7.40±2.22	2.71±0.81	2.23±0.67	3.23±0.97	5.49±1.65
	nRMSE	DeepONet	92.25±27.25	2.94±0.87	2.64±0.78	3.83±1.13	6.79±2.00
		FNO	56.55±14.19	3.00±0.67	3.02±0.60	3.92±0.73	7.09±1.82
		4DHemoFormer	58.72±12.94	88.96±1.38	88.78±1.68	87.64±1.22	86.40±1.17
ECA		PINN	57.47±2.87	82.48±4.12	80.11±4.01	75.52±3.78	62.45±3.12
	Correlation coefficient	DeepONet	54.52±22.49	89.29±23.76	88.92±23.66	89.37±23.79	88.65±23.59
		FNO	56.72±16.74	88.30±14.34	87.80±14.21	88.10±19.45	87.77±12.96
		4DHemoFormer	9.27±2.78	0.63±0.09	0.61±0.09	0.82±0.14	1.40±0.22
		PINN	10.26±3.08	2.68±0.80	2.27±0.68	2.74±0.82	5.02±1.51
	nRMSE	DeepONet	42.85±8.11	0.94±0.17	0.97±0.14	1.75±0.19	2.53±0.66
		FNO	28.52±3.80	1.44±0.19	1.70±0.23	2.13±0.28	3.27±0.44
		4DHemoFormer	81.05±5.39	96.85±0.66	96.83±0.68	96.84±0.46	96.51±0.46
VA		PINN	80.90±4.05	95.69±0.13	94.73±0.14	94.25±0.40	91.61±4.58
	Correlation coefficient	DeepONet	84.12±13.73	86.06±9.74	86.06±25.77	85.89±9.08	85.76±17.38
		FNO	62.63±13.69	84.80±18.53	84.51±18.47	84.47±18.46	84.19±18.40

Supplementary Table 3. Prediction Performance (mean+/-std) for multi-step prediction task on temporal extrapolation

Vessel Site	**Metrics**	**Models**	**p (10^{-2})**	**u(10^{-2})**	**v(10^{-2})**	**w(10^{-2})**	**velocity magnitude (10^{-2})**
		4DHemoFormer	266.73±264.40	6.07±3.50	5.51±3.30	9.27±5.55	13.28±8.17
		PINN	468.15±774.17	7.93±4.13	7.40±4.46	11.80±9.29	17.49±10.86
	nRMSE	DeepONet	796.03±558.84	9.24±3.66	9.57±3.48	16.14±7.81	25.32±12.68
Overall		FNO	831.98±681.02	10.18±3.68	10.41±4.78	18.31±9.59	28.59±16.92
		4DHemoFormer	66.95±13.85	94.85±3.56	95.14±3.56	97.38±2.45	97.36±2.36
	Correlation	PINN	75.25±37.82	94.58±6.98	94.83±7.00	96.54±2.97	95.66±2.78

	coefficient	DeepONet	62.15±23.46	93.23±4.57	93.37±4.38	94.58±3.99	94.37±3.27
		FNO	59.34±12.57	91.85±4.56	91.14±4.56	93.53±3.99	92.48±3.25
		4DHemoFormer	781.91±813.43	8.75±4.80	8.31±4.05	16.68±9.10	19.41±11.06
		PINN	1628.00±1481.50	12.72±5.20	12.60±5.43	24.86±10.91	30.31±13.64
	nRMSE	DeepONet	1981.96±1843.38	12.55±4.28	13.54±4.15	27.72±8.95	37.29±17.61
CCA		FNO	2056.48±1628.30	13.44±4.50	14.75±5.62	32.00±9.56	42.72±16.40
		4DHemoFormer	7.75±18.38	85.52±10.23	86.42±10.32	94.38±6.74	94.32±6.65
	Correlation coefficient	PINN	19.11±33.77	84.16±8.38	84.36±8.56	92.22±5.28	91.53±6.91
		DeepONet	17.58±17.46	82.39±9.83	82.03±9.06	90.96±6.14	90.14±6.15
		FNO	16.41±27.77	81.22±9.19	83.11±10.14	87.47±5.03	87.08±6.74
		4DHemoFormer	27.77±22.82	3.81±1.96	3.39±2.07	6.22±3.88	8.15±5.17
	nRMSE	PINN	35.45±36.20	5.43±2.93	4.97±2.84	7.61±4.83	11.68±7.57
		DeepONet	41.31±26.54	5.39±1.27	5.58±1.30	8.51±3.54	13.69±4.45
		FNO	44.52±23.61	5.96±1.15	6.06±2.04	9.05±3.73	15.55±5.29
ICA		4DHemoFormer	93.59±10.52	97.62±1.86	98.16±1.40	98.17±1.35	98.59±0.98
	Correlation coefficient	PINN	97.59±6.88	97.42±1.88	98.07±1.48	97.28±1.94	97.59±1.82
		DeepONet	91.73±8.47	93.88±1.86	92.09±1.41	94.98±1.59	94.80±1.27
		FNO	84.54±6.34	87.46±1.86	91.10±1.36	92.52±1.79	92.31±1.58
		4DHemoFormer	194.53±164.00	8.75±5.67	7.54±5.50	9.47±6.61	18.50±12.03
	nRMSE	PINN	128.99±84.61	9.90±5.25	9.41±5.05	11.32±6.29	22.09±12.02
		DeepONet	149.39±71.60	10.18±5.03	10.22±5.18	12.22±6.85	26.14±18.05
ECA		FNO	167.56±83.38	11.60±5.58	11.07±5.14	13.58±6.53	28.68±13.04
		4DHemoFormer	80.41±16.00	97.29±1.41	96.99±1.76	97.80±1.15	97.34±1.23
	Correlation coefficient	PINN	86.34±13.47	97.67±1.41	97.84±1.54	97.67±1.43	96.83±1.97
		DeepONet	74.16±14.55	92.23±1.41	97.77±1.74	93.72±1.05	92.91±1.33
		FNO	72.85±13.19	97.47±1.41	94.32±1.63	92.80±1.18	91.96±1.19
		4DHemoFormer	62.70±57.34	2.96±1.57	2.79±1.58	4.69±2.61	7.08±4.42
	nRMSE	PINN	80.17±36.65	3.66±1.15	2.63±1.20	3.41±1.69	5.90±2.11
		DeepONet	90.67±32.04	3.56±1.66	2.86±1.07	3.96±1.26	7.13±2.51
		FNO	109.09±47.92	4.11±1.17	3.14±1.44	4.52±1.28	8.13±2.60
VA		4DHemoFormer	86.05±10.49	98.99±0.74	98.97±0.76	99.17±0.55	99.19±0.58
	Correlation coefficient	PINN	97.98±2.35	99.07±0.80	99.05±0.82	98.99±0.84	96.68±1.28
		DeepONet	77.06±3.71	89.02±0.74	92.03±0.82	93.08±0.59	87.63±0.63
		FNO	72.14±3.50	82.05±0.79	89.00±0.78	90.08±0.77	90.10±0.76

Supplementary Table 4. Prediction Performance (mean+/-std) for single-step prediction task on cross-geometry generalization

Vessel Site	Metrics	Models	p (10^{-2})	u(10^{-2})	v(10^{-2})	w(10^{-2})	velocity magnitude (10^{-2})
Overall	nRMSE	4DHemoFormer	8.25±2.24	0.93±0.24	0.81±0.23	1.65±0.45	2.39±0.56
		PINN	12.62±5.29	3.54±0.50	3.43±0.47	5.25±2.06	7.34±1.81
		DeepONet	89.19±19.11	2.42±0.44	2.43±0.41	7.90±1.34	8.85±1.74
		FNO	165.46±34.29	5.40±0.87	6.09±0.86	7.94±1.12	10.46±2.46
	Correlation coefficient	4DHemoFormer	70.09±23.14	89.46±6.19	90.73±6.14	89.33±4.44	88.95±5.09
		PINN	67.67±12.55	68.92±22.64	69.84±21.49	74.88±10.43	59.07±14.88
		DeepONet	69.07±13.06	85.08±13.41	84.87±14.39	84.44±11.23	84.28±14.36
		FNO	31.85±4.31	72.18±10.11	71.17±10.81	77.70±11.16	75.51±9.64
T1: VA-CG	nRMSE	4DHemoFormer	8.32±2.19	0.95±0.35	0.88±0.34	1.77±0.75	2.34±0.88
		PINN	13.26±2.39	4.17±0.42	3.98±1.05	7.44±0.98	10.34±2.70
		DeepONet	34.02±4.67	1.27±0.27	1.36±0.39	2.77±0.57	3.87±0.50
		FNO	69.32±16.59	2.09±0.59	2.52±0.73	3.59±0.52	5.02±1.20
	Correlation coefficient	4DHemoFormer	55.93±30.45	85.66±12.06	85.66±10.40	85.16±7.86	85.19±8.46
		PINN	71.04±1.49	68.48±0.92	68.31±6.50	76.33±3.59	45.13±6.83
		DeepONet	54.84±6.43	77.11±24.78	76.93±24.55	77.11±25.42	76.29±24.74
		FNO	40.40±4.41	75.16±18.98	73.98±13.52	73.42±10.21	73.54±12.76
T2: CCA-CG	nRMSE	4DHemoFormer	6.16±4.51	1.00±0.21	0.63±0.24	1.22±0.31	1.67±0.56
		PINN	19.95±5.79	3.52±0.78	4.19±1.00	8.42±1.45	7.52±1.21
		DeepONet	219.77±56.61	3.34±0.94	3.23±0.68	9.61±2.38	10.17±1.57
		FNO	507.12±90.14	4.98±0.91	4.46±1.25	7.42±1.37	8.13±2.26
	Correlation coefficient	4DHemoFormer	65.71±20.73	88.36±2.87	89.99±2.81	88.54±1.46	87.57±4.60
		PINN	51.18±2.14	52.80±1.47	37.61±2.16	60.97±1.01	57.41±2.14
		DeepONet	57.94±6.22	83.41±16.13	83.41±11.18	85.42±14.62	85.34±11.66
		FNO	28.47±3.42	82.97±10.96	80.97±12.71	83.87±16.85	83.84±20.38
T3: ECA_CG	nRMSE	4DHemoFormer	7.30±1.30	0.88±0.32	0.83±0.27	1.69±0.65	1.94±0.70
		PINN	15.98±1.44	3.37±0.90	3.24±0.83	4.34±0.91	7.80±2.06
		DeepONet	37.53±9.35	2.55±0.68	2.40±0.25	5.49±1.37	8.32±0.84
		FNO	161.17±46.55	3.64±0.78	5.27±0.96	7.21±2.08	9.34±1.84
	Correlation	4DHemoFormer	75.28±35.85	90.29±10.7	89.77±11.10	90.46±8.2	90.64±8.55

	coefficient			4		4	
		PINN	60.55±17.64	71.28±7.59	67.22±7.45	73.43±4.75	55.21±9.19
		DeepONet	70.06±14.29	86.85±20.06	86.30±13.09	85.76±15.58	84.64±21.52
		FNO	35.45±8.20	83.45±15.66	84.82±23.73	80.43±19.57	86.80±24.70
		4DHemoFormer	10.17±1.71	0.85±0.34	0.96±0.32	1.98±0.74	2.85±0.83
	nRMSE	PINN	7.04±4.14	3.82±1.04	2.87±0.78	4.12±0.96	7.02±1.88
		DeepONet	11.66±2.04	1.81±0.33	1.45±0.15	3.05±0.88	3.71±0.55
		FNO	36.85±4.50	7.54±1.21	7.40±2.16	8.42±1.49	12.31±2.69
		4DHemoFormer	68.57±46.79	87.50±10.45	86.93±10.83	87.40±7.95	86.80±7.92
T4: ICA_CG		PINN	80.42±6.51	83.92±2.84	81.47±5.00	70.96±6.38	61.45±5.76
	Correlation	DeepONet	55.61±23.87	76.24±13.16	77.18±18.45	76.24±19.58	76.44±10.38
		FNO	34.46±10.01	70.15±11.09	59.85±11.86	75.56±14.80	65.71±15.89
		4DHemoFormer	7.22±2.54	0.90±0.34	0.82±0.28	2.14±0.63	3.18±0.70
		PINN	15.27±3.37	3.09±0.34	3.60±0.93	7.33±1.13	8.90±0.97
	nRMSE	DeepONet	119.18±16.75	2.28±0.32	2.07±0.29	18.02±2.53	14.79±2.08
		FNO	125.92±16.40	7.72±1.35	7.87±2.01	10.15±1.18	10.85±1.54
		4DHemoFormer	75.45±25.17	82.38±11.06	91.70±10.91	82.07±7.77	84.01±8.67
T5: CCA_CS		PINN	63.49±5.26	21.84±21.74	40.87±29.83	61.28±18.46	33.58±26.63
	Correlation coefficient	DeepONet	68.17±14.57	85.61±17.82	84.42±17.60	85.83±17.86	85.19±17.74
		FNO	19.98±5.99	42.14±12.62	52.55±15.74	86.57±25.93	77.68±23.27
		4DHemoFormer	3.45±0.95	0.70±0.10	0.67±0.07	0.94±0.12	1.52±0.18
		PINN	3.62±1.09	4.33±1.30	2.86±0.86	3.33±1.00	6.23±1.87
	nRMSE	DeepONet	3.68±0.39	1.24±0.19	0.73±0.19	2.13±0.28	2.12±0.37
		FNO	10.88±1.82	2.18±0.52	1.47±0.39	4.66±0.96	3.41±0.47
		4DHemoFormer	89.36±1.33	96.33±0.87	96.29±1.09	96.63±0.92	96.69±0.61
T6: ICA_CS		PINN	86.59±4.33	74.34±6.77	89.60±0.97	85.54±4.28	70.43±3.52
	Correlation coefficient	DeepONet	76.56±24.01	87.03±24.13	87.18±24.16	87.53±24.25	86.91±24.10
		FNO	63.72±8.50	85.11±12.6	85.09±12.68	84.89±11.	73.77±12.51

				9		32	
	nRMSE	4DHemoFormer	9.20±3.28	1.18±0.19	0.85±0.18	1.63±0.21	2.93±0.39
		PINN	12.86±1.32	3.02±1.03	3.22±0.96	3.30±0.89	7.14±1.70
		DeepONet	87.64±11.79	3.28±0.37	3.23±0.41	4.97±0.72	9.27±0.98
		FNO	53.37±9.24	4.91±0.60	7.09±2.01	7.73±0.94	12.34±3.03
T7: ECA_CS	Correlation coefficient	4DHemoFormer	61.00±4.99	88.36±1.05	88.56±1.49	88.74±0.93	85.44±1.44
		PINN	57.91±9.31	82.77±0.99	78.44±2.63	76.08±1.36	61.08±2.90
		DeepONet	55.98±14.23	76.38±9.84	87.07±21.81	86.89±26.54	85.32±17.59
		FNO	23.87±4.58	73.06±17.85	81.98±15.73	83.91±16.10	83.29±15.98
	nRMSE	4DHemoFormer	14.15±1.43	0.96±0.10	0.89±0.11	1.86±0.18	2.71±0.26
		PINN	12.95±2.34	3.00±0.98	3.49±0.46	3.76±0.69	3.76±1.67
		DeepONet	25.01±5.74	1.45±0.19	3.08±0.90	3.54±0.99	6.48±1.26
		FNO	57.92±9.12	6.40±1.37	8.56±0.73	9.81±2.39	13.88±2.05
T8: VA_CS	Correlation	4DHemoFormer	69.46±19.77	96.83±0.46	96.92±0.50	96.62±0.42	96.28±0.43
		PINN	70.18±1.40	95.91±0.19	95.17±0.12	94.46±0.46	88.26±5.61
		DeepONet	69.30±12.90	97.04±14.02	95.83±13.84	96.33±13.92	86.30±13.91
		FNO	39.77±11.21	51.84±14.71	39.64±4.54	39.55±4.23	29.10±2.92

Supplementary Table 5. Prediction Performance (mean+/-std) for multi-step prediction task on cross-geometry generalization

Vessel Site	**Metrics**	**Models**	**p (10^{-2})**	**u(10^{-2})**	**v(10^{-2})**	**w(10^{-2})**	**velocity magnitude (10^{-2})**
Overall	nRMSE	4DHemoFormer	180.73±174.73	6.10±3.77	6.30±3.61	10.23±6.27	13.61±8.26
		PINN	310.94±476.35	7.76±4.33	7.26±4.50	11.26±9.06	16.23±9.60
		DeepONet	409.42±356.45	8.65±3.56	9.68±3.81	16.10±6.86	22.00±7.66
		FNO	435.20±252.65	9.32±4.31	10.84±4.42	17.31±7.90	24.73±8.55
	Correlation coefficient	4DHemoFormer	51.37±15.04	81.89±4.86	82.01±4.19	84.68±2.84	84.33±3.36
		PINN	81.93±25.57	95.13±6.21	95.38±6.00	96.99±2.40	96.11±2.17
		DeepONet	63.89±19.48	82.10±5.62	81.81±4.25	81.87±3.78	82.67±4.43

T1: VA-CG	nRMSE	FNO	63.81±23.85	86.27±5.56	87.41±5.54	85.86±4.69	87.76±3.76
		4DHemoFormer	224.85±265.58	6.88±4.18	7.11±4.40	12.53±8.80	15.96±10.93
		PINN	50.40±0.69	2.63±0.25	2.87±0.17	3.78±0.15	6.26±0.22
		DeepONet	62.20±32.61	2.56±1.96	3.10±1.38	4.36±2.73	7.83±3.18
		FNO	64.70±23.46	2.79±1.46	3.31±1.06	4.74±2.25	8.18±4.53
		4DHemoFormer	44.93±17.44	92.88±5.50	92.68±5.01	96.05±2.95	96.10±3.00
	Correlation coefficient	PINN	98.13±0.25	99.08±0.04	98.98±0.15	98.97±0.03	98.31±0.53
		DeepONet	61.99±7.95	88.12±4.78	90.66±0.14	89.31±2.42	93.69±2.34
		FNO	56.62±0.24	93.02±3.45	87.76±1.56	92.36±0.03	94.05±2.51
		4DHemoFormer	69.05±49.86	4.62±2.04	4.35±1.60	7.44±3.79	11.50±5.92
T2: CCA-CG	nRMSE	PINN	1167.50±515.89	14.57±5.58	14.31±4.46	26.47±7.60	31.82±9.49
		DeepONet	1207.35±96.52	11.99±6.71	17.62±6.76	31.08±9.84	33.85±9.59
		FNO	1819.12±84.41	13.12±7.45	19.78±5.16	31.85±9.82	37.44±9.46
		4DHemoFormer	7.40±15.51	93.93±3.44	95.24±2.53	94.72±2.39	93.11±2.87
	Correlation coefficient	PINN	48.35±22.42	85.35±5.60	86.93±5.22	93.60±2.78	92.92±3.29
		DeepONet	55.46±14.24	80.01±3.67	90.79±2.32	91.04±2.65	90.10±2.68
		FNO	35.62±20.27	86.75±5.52	87.79±2.64	88.47±2.59	85.05±3.12
		4DHemoFormer	237.10±240.54	6.53±4.14	6.42±3.54	11.23±6.74	12.72±6.83
T3: ECA_CG	nRMSE	PINN	159.28±92.94	10.72±4.74	9.51±4.33	11.64±5.19	22.34±10.55
		DeepONet	183.13±82.08	10.96±5.85	10.11±5.46	12.91±4.25	27.64±9.95
		FNO	204.42±95.19	11.66±7.99	11.49±6.56	13.98±5.78	30.11±18.46
		4DHemoFormer	63.02±10.39	91.31±7.15	90.44±5.84	95.89±2.93	94.64±4.12
	Correlation coefficient	PINN	92.76±5.70	97.64±0.73	97.50±1.10	97.65±0.86	96.16±1.15
		DeepONet	62.79±6.58	90.41±3.26	85.03±1.16	93.07±2.32	92.90±3.86
		FNO	61.54±10.37	87.73±0.91	83.05±3.56	91.36±0.82	90.81±2.74
		4DHemoFormer	376.38±363.26	7.18±5.01	7.65±5.02	13.12±8.93	17.37±12.08
T4: ICA_CG	nRMSE	PINN	32.85±8.58	5.50±0.88	4.55±0.64	7.11±1.26	10.88±1.50
		DeepONet	47.74±10.13	3.55±1.31	3.78±1.81	7.25±4.14	5.78±2.99
		FNO	52.51±13.52	4.14±1.48	4.37±1.82	8.29±4.86	6.39±3.67
		4DHemoFormer	71.20±13.68	94.08±4.65	94.19±4.95	96.87±2.57	96.76±2.61
	Correlation	PINN	93.11±4.33	97.28±0.58	97.58±0.94	97.19±0.65	96.79±1.11
		DeepONet	75.39±9.70	92.97±4.01	93.50±3.77	93.06±2.38	92.78±2.19
		FNO	73.11±11.68	85.73±0.55	92.43±0.92	91.92±0.94	90.78±2.08
		4DHemoFormer	283.83±282.60	8.33±6.25	10.51±6.64	16.18±9.26	16.32±9.08
T5: CCA_CS	nRMSE	PINN	876.50±768.02	10.08±4.82	10.30±5.10	21.67±10.38	22.46±11.70
		DeepONet	1025.23±245.	10.27±4.26	11.14±5.39	24.88±8.94	26.96±8.77

			35				
		FNO	1447.03±264.25	10.92±5.85	12.01±6.88	27.50±9.53	32.89±9.53
		4DHemoFormer	5.34±20.36	84.62±14.82	86.34±10.73	92.66±7.63	91.22±8.72
	Correlation coefficient	PINN	34.09±40.65	85.63±1.11	85.81±9.09	92.42±5.06	92.22±6.56
		DeepONet	41.62±19.76	75.18±14.40	83.86±10.20	90.45±6.65	83.02±8.29
		FNO	36.65±18.53	83.03±6.48	82.10±9.21	88.60±7.27	92.17±8.04
		4DHemoFormer	25.24±18.34	3.62±2.13	2.88±1.50	4.62±2.84	6.58±4.08
	nRMSE	PINN	26.29±26.77	4.16±1.95	3.28±1.58	4.69±2.26	7.34±3.61
		DeepONet	30.76±10.26	4.23±1.12	3.52±1.30	5.24±2.42	9.06±4.69
T6: ICA_CS		FNO	34.93±9.55	4.34±0.96	3.86±0.99	5.55±2.51	10.03±3.35
		4DHemoFormer	96.89±1.99	98.38±0.84	98.23±1.21	98.41±0.87	98.63±0.54
	Correlation coefficient	PINN	99.32±0.77	99.04±0.33	99.17±0.34	98.91±0.46	98.90±0.43
		DeepONet	90.38±1.42	95.86±0.58	93.74±0.53	95.55±0.68	93.69±0.52
		FNO	91.98±0.83	92.73±0.34	96.07±0.39	92.45±0.45	90.68±0.46
		4DHemoFormer	183.97±148.47	8.42±5.30	8.39±4.83	10.95±7.90	20.21±13.91
	nRMSE	PINN	117.05±64.39	9.98±5.40	9.71±5.43	10.46±5.33	19.95±9.97
		DeepONet	139.52±52.30	10.33±6.46	10.30±5.58	11.36±7.85	23.92±16.89
T7: ECA_CS		FNO	157.57±50.33	11.09±4.01	12.05±5.09	12.50±7.69	25.66±11.98
		4DHemoFormer	76.76±11.73	96.74±1.39	95.85±1.95	97.08±1.45	95.92±1.77
	Correlation coefficient	PINN	90.92±7.33	97.82±1.31	97.84±1.42	98.23±1.07	97.08±1.70
		DeepONet	70.90±9.93	94.80±1.29	92.96±1.91	96.74±1.15	93.32±1.75
		FNO	73.85±7.89	92.63±1.35	88.23±1.93	93.10±1.42	92.40±1.71
		4DHemoFormer	45.39±29.15	3.17±1.11	3.07±1.30	5.74±1.90	8.22±3.21
	nRMSE	PINN	57.62±14.41	4.41±1.69	3.51±1.45	4.26±2.04	8.88±3.62
		DeepONet	67.54±21.19	4.44±1.37	3.83±1.67	4.64±1.26	10.77±3.53
		FNO	75.84±37.49	4.81±1.73	4.03±1.44	5.27±1.16	11.90±3.27
T8: VA_CS		4DHemoFormer	80.75±9.39	98.58±0.76	98.92±0.62	99.11±0.51	99.07±0.56
	Correlation	PINN	98.75±1.15	99.18±0.68	99.17±0.69	98.97±0.83	96.23±1.32
		DeepONet	74.40±8.81	92.90±0.69	92.01±0.63	94.09±0.71	92.32±1.26
		FNO	72.66±1.08	87.49±0.73	90.70±0.67	93.35±0.68	91.06±1.04

Supplementary Table 6. Prediction Performance (mean+/-std) of 4DHemoFormer for cross-domain transferability in single-step and multi-step prediction task

Vessel Site	**Metrics**	**Models**	**Metrics**	**u(10^{-2})**	**v(10^{-2})**	**w(10^{-2})**	**velocity magnitude (10^{-2})**
	Zero-shot setting	Single-step	nRMSE	8.19±1.03	7.80±1.19	13.16±2.04	6.28±0.91
			CC	96.72±1.53	90.45±2.06	78.72±5.12	96.43±0.94

Intracranial artery		Multi-step	nRMSE	7.55±1.07	12.34±4.43	15.98±3.92	10.44±2.96
			CC	90.08±3.36	81.37±5.53	68.92±7.00	87.56±6.35
	Fine-tuning setting (10%)	Single-step	nRMSE	2.21±0.66	2.40±0.730	2.45±0.61	3.51±0.88
			CC	98.86±0.79	99.12±0.44	98.56±0.73	97.79±1.08
		Multi-step	nRMSE	5.81±2.16	5.20±1.52	6.64±1.99	7.76±1.25
			CC	91.45±5.73	93.90±3.33	90.13±5.71	89.46±6.10

Supplementary Table 7. Runtime of the models averaged on ICA, ECA, CCA and VA

Single-step prediction task on CFD data					
	Data-driven models				Numerical simulation (each second)
Method	PINN	FNO	DeepONet	4DHemoFormer	-
Training time (hours)	0.4	10.1	50.6	18.5	-
Inference time (seconds)	10.5	0.8	31.4	24.6	415.43*

Multi-step prediction task on CFD data					
	Data-driven models				Numerical simulation (each second)
Method	PINN	FNO	DeepONet	4DHemoFormer	-
Training time (hours)	0.2	12.1	76.0	11.2	-
Inference time (seconds)	8.7	1.0	102.7	23.5	415.43*

Single-step prediction task on in-vivo data					
	Data-driven models				Acquisition time
Method	PINN	FNO	DeepONet	4DHemoFormer	-
Training time (hours)	0.2	40.0	151.8	7.0	-
Inference time (seconds)	2.3	0.8	23.5	4.8	575

Multi-step prediction task on in-vivo data					
	Data-driven models				Acquisition time
Method	PINN	FNO	DeepONet	4DHemoFormer	-
Training time (hours)	0.1	48.0	305.0	7.0	-

Inference time (seconds)	1.8	0.9	77.0	6.5	575

Supplementary Table 8. Parameters settings for 4DHemoFormer and baseline methods

Architecture		**Parameters settings**
4DHemoFormer	Layers	4
	Hidden size	1024
	Optimizer	Adam
	Scheduler	ReduceLROnPlateau
	Number of heads	8
	Dropout rate	0.1
	Learning rate	0.0001
	Physical loss weight (Alpha)	0.5
	Training points	2500 /frames (FPS sampling)
	Testing points	Overall grid (patch based)
PINN	FNN width	128
	FNN depth	4
	Optimizer	Adam
	Learning rate	0.0001
	scheduler	StepLR
	Scheduler step	1000
	Scheduler gamma	0.99
	Physical loss weight (Alpha)	0.5
	Training points	2500 /frames (FPS sampling)
	Testing points	Overall grid
FNO	Layers	4
	Hidden dim	32
	Modes	12,12,12
	Optimizer	Adam
	Learning rate	1e-3
	Scheduler	StepLR
	Scheduler step	20
	Scheduler gamma	0.9
DeepONet	Width	100
	Branch depth	8
	Trunk depth	8
	Optimizer	Adam
	Learning rate	1e-3
	Scheduler	StepLR
	Scheduler step	20
	Scheduler gamma	0.9

References:

[s1]Mons, V., Chassaing, J.-C., Gomez, T. & Sagaut, P. Reconstruction of unsteady viscous flows using data assimilation schemes. *J. Comput. Phys.* 316, 255–280 (2016).

[s2]Asch, M., Bocquet, M. & Nodet, M. *Data Assimilation: Methods, Algorithms, and Applications* (Society for Industrial and Applied Mathematics, 2016).